

Developmental profile and properties of sulforhodamine 101—Labeled glial cells in acute brain slices of rat hippocampus

Karl Wolfgang Kafitz^{1,2}, Silke Doris Meier^{1,3}, Jonathan Stephan^{1,4},
Christine Rosemarie Rose*

Institut für Neurobiologie, Heinrich-Heine-Universität Düsseldorf, Universitätsstrasse 1, D-40225 Düsseldorf, Germany

Received 30 August 2007; received in revised form 23 November 2007; accepted 26 November 2007

Abstract

The reliable identification of astrocytes for physiological measurements was always time-consuming and difficult. Recently, the fluorescent dye sulforhodamine 101 (SR101) was reported to label cortical glial cells *in vivo* [Nimmerjahn A, Kirchhoff F, Kerr JN, Helmchen F. Sulforhodamine 101 as a specific marker of astroglia in the neocortex *in vivo*. *Nat Methods* 2004;1:31–7]. We adapted this technique for use in acute rat hippocampal slices at early postnatal stages (P3, 7, 15) and in young adults (P24–27) and describe a procedure for double-labeling of SR101 and ion-selective dyes. Using whole-cell patch-clamp, imaging, and immunohistochemistry, we characterized the properties of SR101-positive versus SR101-negative cells in the *stratum radiatum*. Our data show that SR101, in contrast to Fura-2 or SBFI, only stains a subset of glial cells. Throughout development, SR101-positive and SR101-negative cells differ in their basic membrane properties. Furthermore, SR101-positive cells undergo a developmental switch from variably rectifying to passive between P3 and P15 and lack voltage-gated Na⁺ currents. At P15, the majority of SR101-positive cells is positive for GFAP. Thus, our data demonstrate that SR101 selectively labels a subpopulation of glial cells in early juvenile hippocampi that shows the typical developmental changes and characteristics of classical astrocytes. Owing to its reliability and uncomplicated handling, we expect that this technique will be helpful in future investigations studying astrocytes in the developing brain.
© 2007 Elsevier B.V. All rights reserved.

Keywords: Astrocyte; Sulforhodamine 101; Hippocampus; Imaging; Electrophysiology; GFAP; SBFI; Fura-2

1. Introduction

During the last decade it has been firmly established that astrocytes are not purely supportive for neuronal function, but also modulate the synaptic communication between neurons (Araque et al., 1999; Fiacco et al., 2007; Haydon, 2001; Haydon and Carmignoto, 2006; Kang et al., 1998; Nedergaard, 1994; Newman and Volterra, 2004; Parri et al., 2001; Parri and Crunelli, 2007; Pascual et al., 2005; Schipke and Kettenmann, 2004; Serrano et al., 2006; Verkhratsky et al., 1998; Volterra

and Meldolesi, 2005). Recent studies demonstrated that astroglia also plays a central role in the regulation of blood vessel diameter during neuronal activity (Metea and Newman, 2006; Mulligan and MacVicar, 2004; Takano et al., 2006; Zonta et al., 2003). The analysis of astrocytes in the intact tissue with electrophysiological and high-resolution imaging techniques, however, was always hampered by the problem of a reliable identification of this cell type. The identification of astrocytes based solely on morphological criteria, such as somatic size and cellular architecture, hosts the chance to mistakenly include small-sized neurons (Kimelberg, 2004). Immunohistochemical stainings of markers such as glial fibrillary acidic protein (GFAP) or the Ca²⁺-binding protein S-100 β can only be performed after the experiment, are time-consuming and often do not allow an undeniable identification of the cells analyzed in physiological experiments. To overcome this problem, transgenic mice, in which enhanced green fluorescent protein (EGFP) is expressed under the human GFAP promoter have been raised (Hirrlinger et al., 2006; Nolte et al., 2001; Zhuo et al., 1997). However, because astrocytes show very diverse levels of GFAP-expression

* Corresponding author. Tel.: +49 211 81 13416; fax: +49 211 81 13415.

E-mail addresses: kafitz@uni-duesseldorf.de (K.W. Kafitz), s.meier@uni-duesseldorf.de (S.D. Meier), jonathan.stephan@uni-duesseldorf.de (J. Stephan), rose@uni-duesseldorf.de (C.R. Rose).

¹ These authors equally contributed to this study.

² Tel.: +49 211 81 13486.

³ Tel.: +49 211 81 10581.

⁴ Tel.: +49 211 81 10582.

(Kimmelberg, 2004), this approach enables the identification of only a subset of astrocytes.

Many studies reported that glial cells take up the membrane-permeable forms of Ca^{2+} indicator dyes such as Fura-2 or Fluo-4 much better than neurons (Dallwig and Deitmer, 2002; Wang et al., 2006), and astrocytes were thus often identified based on the emission patterns of the indicator dyes used. This approach was extended by Dallwig and Deitmer (2002), who have described that neurons and astrocytes in acute brain slices differ in their response to changes in the external potassium concentration. Still, this approach can only identify about 80% of astrocytes and necessitates performing additional Ca^{2+} -imaging experiments.

Recently, the fluorescent dye sulforhodamine 101 (SR101) was reported as a powerful tool for specific labeling of cortical glial cells in the intact brain of juvenile and adult rodents (Nimmerjahn et al., 2004; Wang et al., 2006). In the present study we adapted this technique for use in an acute tissue slice preparation of the rat hippocampus. Because in the CA1 region of the rodent hippocampus, astrocytes undergo considerable changes in channel complement and passive membrane properties during postnatal development (Bordey and Sontheimer, 1997; Kressin et al., 1995; Zhou et al., 2006), we performed the study at different developmental stages during the first 4 weeks after birth (postnatal days 3, 7, 15, and 24–27). Using whole-cell patch-clamp, imaging techniques, and immunohistochemistry, we show that the percentage of SR101-positive cells in the *stratum radiatum* increases during development. Furthermore, SR101-positive cells lack voltage-gated Na^+ currents and change from variably rectifying to passive cells between P3 and P15. At P15, the majority of SR101-labeled cells is positive for the astrocytic marker GFAP. Thus, our data demonstrate that SR101 selectively labels a subset of glial cells in the hippocampus that shows typical characteristics of classical astrocytes.

2. Methods

2.1. Tissue preparation and labeling with SR101

Experiments were carried out on acute tissue slices (250 μm) of rat hippocampi harvested at postnatal days 3, 7, 15, and 24–27 as described earlier (Meier et al., 2006). In brief, animals were decapitated and the hippocampi were rapidly removed. Slices of P3 and P7 animals were sectioned in ice-cold normal artificial cerebrospinal fluid (ACSF; in mM: 125 NaCl, 2.5 KCl, 2 CaCl_2 , 1 MgCl_2 , 1.25 NaH_2PO_4 , 26 NaHCO_3 and 20 glucose, bubbled with 95% O_2 and 5% CO_2 ; pH 7.4). Following sectioning, slices were kept at 34 °C for 20 min in ACSF that contained 0.5–1 μM sulforhodamine 101 (SR101), followed by a 10 min incubation in normal ACSF at 34 °C. Preparation of slices from animals older than 15 days as well as their incubation with SR101 at high temperature was performed in ACSF with a reduced Ca^{2+} concentration (in mM: 125 NaCl, 2.5 KCl, 0.5 CaCl_2 , 6 MgCl_2 , 1.25 NaH_2PO_4 , 26 NaHCO_3 and 20 glucose, bubbled with 95% O_2 and 5% CO_2 ; pH 7.4). Afterwards, all slices were kept at room temperature until they were used for experiments, which were also performed at room temperature. Unless stated oth-

erwise, all chemicals were purchased from Sigma–Aldrich Co. (Taufkirchen, Germany).

2.2. Determination of the density of SR101-labeled cells

For determination of the amount of SR101-positive cells on the total number of cells exhibiting glial morphology, slices were double-labeled with SR101 and the ester form of sodium-binding benzofuran isophthalate (SBFI), a conventional Na^+ -selective fluorescent dye that exhibits similar properties as Fura-2 (Meier et al., 2006). To this end, SBFI-AM (800 μM) was repeatedly (1–5 s duration each) pressure-injected through a fine-tipped glass microelectrode into the *stratum radiatum* (Stosiek et al., 2003). Injection was followed by a 45–60 min wash in normal ACSF at room temperature to allow for diffusion and de-esterification of the dye. Stacks of images (31 optical sections at 1 or 1.5 μm thickness) were then taken at a custom build two-photon laser scanning microscope (excitation wavelength at 850 nm) based on an Olympus FV300 system (Olympus Europe, Hamburg, Germany), coupled to a Mai-Tai Broadband laser (Spectra Physics, Darmstadt, Germany) and equipped with two fluorescence detection channels. Fluorescence emission of SBFI was collected between 400 and 590 nm, emission of SR101 was detected between 610 and 630 nm. Maximum intensity projections and analyses of the staining patterns were performed at montages of image stacks using “ImageJ”-software.

2.3. Electrophysiology and immunohistochemistry

Somatic whole-cell recordings were obtained at an upright microscope (Nikon Eclipse E600FN, 60 \times water immersion objective, N.A. 1.00, Nikon Europe, Düsseldorf, Germany) using an EPC10 amplifier (HEKA Elektronik, Lambrecht, Germany). “PatchMaster”-software (HEKA Elektronik) was used for data acquisition. Some recordings were carried out at a Zeiss AxioScope (Zeiss, Jena Germany, 40 \times water immersion objective, N.A. 0.80, Olympus Europe, Hamburg, Germany) using an Axopatch 200A and “PCLamp 8.2”-software for data acquisition (Molecular Devices, Sunnyvale, CA). The pipette solution contained (in mM): 120 K-MeSO₃ or K-gluconate, 32 KCl, 10 HEPES (*N*-(2-hydroxyethyl)piperazine-*N'*-(2-ethanesulfonic acid), 4 NaCl, 4 Mg-ATP and 0.4 Na₃-GTP, 0.1 Alexafluor 488 (Molecular Probes/Invitrogen, Karlsruhe, Germany), pH 7.30. Cells were generally held at membrane potentials of –85 mV. To separate passive conductances from voltage-gated currents, online leak subtraction (P/4) was performed. Data were processed and analyzed by employing “IGOR Pro”-Software (WaveMetrics, Inc., Lake Oswego, OR).

Following electrophysiological recordings, images of fluorescence emission of SR101-labeled (excitation wavelength: 587 nm, emission detected above 602 nm) and Alexa-filled (excitation wavelength: 488 nm, emission detected between 495 and 575 nm) cells were captured by a CCD camera (Spot RT KE, Diagnostic Instruments, Inc., Sterling Heights, MI) and “Spot”-software attached to the microscope. Slices were immediately fixed over night at 4 °C in paraformaldehyde and immuno-

histochemically processed for GFAP (dilution 1:100; DAKO Z0334, Hamburg, Germany) as reported earlier (Kafitz and Greer, 1998; Kafitz et al., 1999). Labeled slices were coverslipped and documented as described above. Images of the immunohistochemistry were corrected for shrinkage caused by fixation by a factor of 1.467 and overlaid employing “Adobe Photoshop”-software.

2.4. Ca^{2+} imaging

Conventional, wide-field fluorescence imaging was performed using a variable scan digital imaging system (TILL Photonics, Martinsried, Germany) attached to an upright microscope (Axioskop, Zeiss, Jena, Germany; 40 \times water immersion objective, N.A. 0.80, Olympus Europe, Hamburg, Germany) and a CCD camera as a sensor (TILL Imago SVGA, TILL Photonics, Martinsried, Germany). To this end, after confirmation of successful SR101-staining (excitation wavelength: 575 nm; detection of emission: >590 nm), cells were additionally dye-loaded with the Ca^{2+} -selective dye Fura-2 (Fura-2-AM, 500 μ M); employing the protocol described above for SBFI.

For wide-field imaging of Fura-2, background-corrected fluorescence signals (>410 nm) were collected from defined regions of interest after alternate excitation at 356 and 380 nm; images were acquired at 2 Hz. After background subtraction, the ratio of the fluorescence emission (F_{356}/F_{380}) was calculated using TillVision software (TILL Photonics, Martinsried, Germany) and data were analyzed off-line using “IGOR Pro”-Software (WaveMetrics, Inc., Lake Oswego, OR). Changes in calcium concentration were estimated based on an *in vitro* calibration of the Fura-2 fluorescence. ATP was applied by a Picospritzer II (General Valve/Parker Hanfin, Flein/Heilbronn, Germany) coupled to standard micropipettes (Hilgenberg, Waldkappel, Germany) placed at a distance of approximately 10–20 μ m to a given cell.

2.5. Statistics

Unless otherwise specified, data are expressed as means \pm S.E.M. Data were statistically analyzed by a standard *t*-test.

3. Results

3.1. Labeling pattern of acute hippocampal slices with SR101 and SR101/SBFI-AM

Incubation of cells in solutions containing 10–20 μ M of the membrane-permeable acetoxymethyl ester (AM) forms of ion-selective fluorescent dyes such as the Ca^{2+} -sensitive dye Fura-2 or the Na^{+} -sensitive dye SBFI enables the loading and analysis of many cells at a time (e.g. Rose and Ransom, 1996, 1997). In acute brain slices, it was observed consistently that this staining protocol results in a fairly selective staining of astrocytes, and consequently, their primary identification in the intact tissue was often based on this specific staining pattern (Dallwig and Deitmer, 2002; Wang et al., 2006). Using bolus loading (injec-

tion of the AM-form of fluorescent dyes into the extracellular space) instead of bath incubation, in contrast, results in a good quality staining of neurons as well as astroglia (Meier et al., 2006; Stosiek et al., 2003). Injection of dyes thus enables the study of both astrocytes and neurons at the same time. However, dye-loaded neurons, such as interneurons with small somata in the *stratum radiatum* of the hippocampus, might be falsely identified as astrocytes based on this staining technique.

To overcome this problem, we adapted a protocol for application of the red fluorescent dye SR101, which was reported to stain astrocytes in the intact cortex of rodents (Nimmerjahn et al., 2004), for use in acute slices of the rat hippocampus. SR101 is excited around 575 nm and its emission can be collected above 590 nm, making it suitable for use in combination with many available ion-selective dyes. Initial experiments were carried out employing a post-incubation with SR101-containing ACSF at room temperature for 20 min. Independent from the SR101 concentration used (from 100 μ M – as suggested by Nimmerjahn et al. (2004) for *in vivo* experiments – down to 0.5 μ M), this protocol resulted in an unspecific surface label of SR101. The vast majority of the unspecific SR101 staining most likely represented a nuclear label of superficial neurons whereas cells with typical astrocytic morphology were not stained (not shown). In stark contrast to this, we found that incubation of the slices right after their preparation in ACSF containing 500 nM–1 μ M SR101 for 20 min at high temperature (34 $^{\circ}$ C), resulted in a highly specific staining of cells with astrocytic morphology that was maintained for more than 8 h. The staining pattern of SR101 in slices obtained from animals at postnatal day 3 (P3, Fig. 1A), P7 (not shown), P15 (Fig. 1B), as well as P24–27 (not shown) excluded virtually all cells of the *stratum pyramidale*, clearly indicating that SR101 exclusively labeled glial cells throughout development in this preparation.

To portray cells additional to SR101-positive ones in these preparations, we performed a second labeling with the Na^{+} -selective fluorescent dye SBFI-AM, which (like Fura-2) is excited in the UV range. SBFI-AM was directly injected into the *stratum radiatum*, followed by a period of 45–60 min incubation in ACSF to allow for diffusion of the dye into the cells and sufficient de-esterification. At all developmental stages investigated (P3, P7, and P15), and in contrast to SR101, SBFI-AM labeled cells in the *stratum pyramidale* (presumably CA1 pyramidal neurons) as well as SR101-negative cells in the *stratum radiatum* with large somata that presumably represented interneurons or ectopic pyramidal neurons (Fig. 1A and B). SBFI-AM labeling in the *stratum radiatum* also included small-sized SR101-negative cells that morphologically resembled astrocytes as judged by the size and shape of their somata and primary processes (Fig. 1A and B). Interestingly, the percentage of SR101-positive cells on the total number of small-sized SBFI-loaded cells with glial morphology changed during postnatal development. At P15 ($n = 757$ cells in 11 slices), roughly 90% of these SBFI-stained cells were also SR101-positive, whereas at P3 ($n = 2185$ cells in 22 slices) only about 50% of them were labeled with SR101 (Fig. 2). As judged by optical inspection of SR101-incubated slices at P24–27 the vast majority of small-sized cells with glial morphology were also SR101-positive.

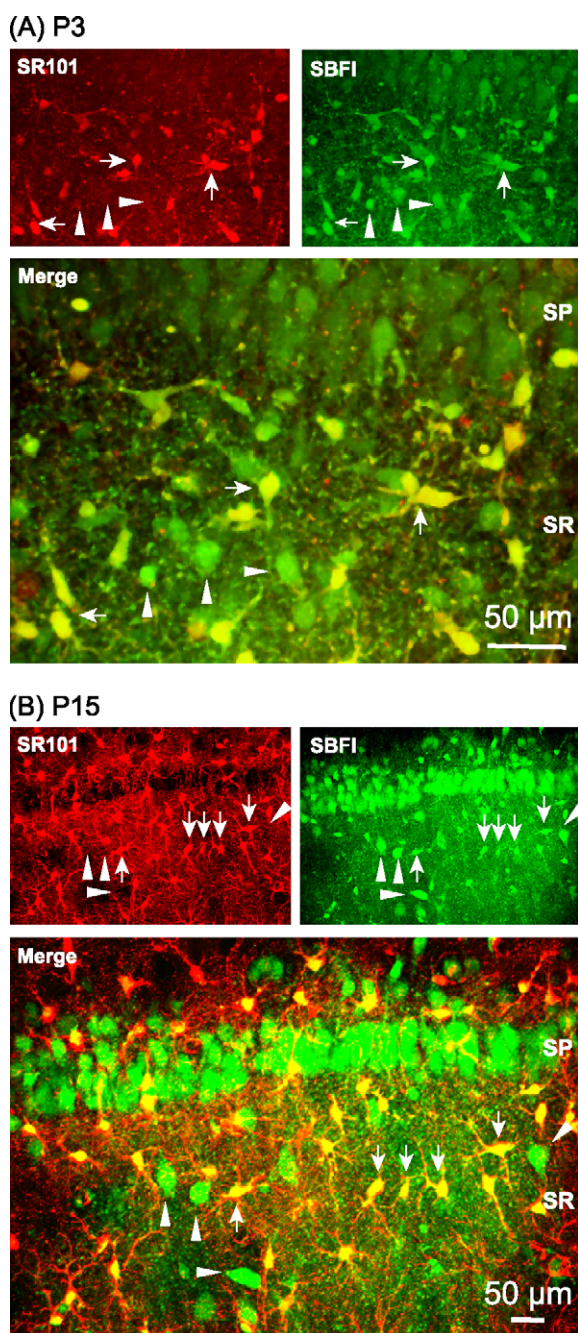


Fig. 1. Labeling pattern of SR101 vs. SBF1-AM in the hippocampal CA1 region. Fluorescence images, taken at a two-photon laser-scanning microscope, of acute slices from postnatal day P3 (A) and P15 (B) rats, double-stained with SR101 (upper left panels) and SBF1-AM (upper right panels). The lower, enlarged panels show the merged fluorescence images. SP: *stratum pyramidale*; SR: *stratum radiatum*. Arrows mark double-labeled cells located in the *stratum radiatum*; arrowheads point out cells which are exclusively stained by SBF1. Note that putative pyramidal neurons in the *stratum pyramidale* are also stained by SBF1, but not with SR101.

Taken together, these results demonstrate that SR101 stains cells with glial morphology in acute tissue slices of the rat hippocampus. Presumptive neurons are completely spared. In addition, we found a clear developmental profile of the staining pattern for SR101. Whereas the SR101-labeling comprised the vast majority of cells with glial morphology in P15 and adult

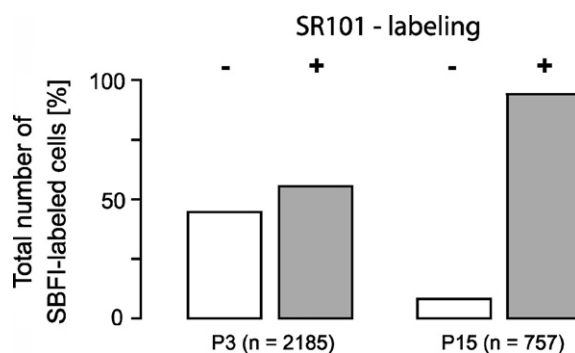


Fig. 2. Quantification of the percentage of SR101-negative (white bars) and SR101-positive (grey bars) cells on the total number of small-sized SBF1-labeled cells located in the *stratum radiatum* in P3 ($n = 22$ slices; 2185 cells) and P15 rats ($n = 11$ slices; 757 cells).

animals, only about half of such cells were stained by SR101 at P3.

3.2. Electrophysiological characterization of SR101-positive and SR101-negative cells

In the CA1 region of the rodent hippocampus, several types of astrocytes were described based on their electrophysiological properties (Bordey and Sontheimer, 2000; D'Ambrosio et al., 1998; Kressin et al., 1995; Steinhäuser et al., 1994b; Zhou and Kimelberg, 2001). Moreover, astrocytes undergo considerable changes in channel complement and passive membrane properties during early postnatal development (Bordey and Sontheimer, 1997; Kressin et al., 1995; Zhou et al., 2006). Therefore, we characterized the electrophysiological properties of SR101-positive and SR101-negative cells with glial morphology in the *stratum radiatum* by performing patch-clamp experiments in the whole-cell configuration. Current injection in the current-clamp mode failed to elicit action potentials in any of the cells investigated ($n = 126$; not shown) indicating that they were indeed glia or glial precursor cells, respectively.

Throughout development, SR101-positive and SR101-negative cells differed significantly in their membrane properties. At early stages, SR101-negative cells ($n = 13$ at P3, $n = 5$ at P15) generally had more depolarized membrane potentials, their membrane resistance was higher and their membrane capacity was lower than that of SR101-positive cells (Table 1). We found no differences in these properties between P3 and P15 animals in SR101-negative cells. At P24–27, SR101-negative cells showed a tendency to be more hyperpolarized and had a higher membrane resistance and capacity compared to younger stages (Table 1). SR101-positive cells also showed developmental changes in their electrophysiological properties. Whereas the membrane potential of SR101-positive cells was highly negative at all four stages investigated (-80 to -87 mV; Table 1), their membrane resistance decreased from 94 M Ω at P3 ($n = 42$), to 68 M Ω at P7 ($n = 6$), and to 6 and 11 M Ω (P15, $n = 37$; P24–27, $n = 13$). At the same time, membrane capacity increased (from 69 to 880 pF; Table 1).

To reveal the functional expression of voltage-gated ion channels, cells were held in the voltage-clamp mode at -85 mV

Table 1
Membrane properties of SR101-positive and SR101-negative cells at P3, P7, P15 and in young adults (P24–27)

SR101 labeling	Age [pnd]	Membrane potential [mV]	Membrane resistance [MΩ]	Membrane capacity [pF]	n
SR-	P3	-67 ± 17	353 ± 325	30 ± 30	13
	P15	-77 ± 14	302 ± 202	27 ± 18	5
	P24-27	-81 ± 5	168 ± 153	95 ± 89	6
SR+	P3	-83 ± 6	94 ± 52	69 ± 48	42
	P7	-80 ± 4	68 ± 32	120 ± 72	6
	P15	-87 ± 3	6 ± 5	139 ± 91	37
	P24-27	-85 ± 4	11 ± 10	880 ± 1274	13

Significance level: ** $\alpha=0.01$.

and then subjected to a rectangular voltage step protocol (from -150 to +50 mV, 10 mV increments). The voltage-step protocol induced large capacitive as well as passive currents (Fig. 3A–C; insets). Leak subtraction (P/4) was performed to reveal voltage-gated currents activated by membrane depolarization (Fig. 3A–C; insets; see also Fig. 4). The amplitudes of the currents were measured at 8–10 ms after the start of the voltage step, and current was plotted versus voltage (*I/V*-relationship, Fig. 3A–C). Data were fit by a linear regression curve; the threshold for linearity of the *I/V* relation was set at a regression coefficient of $r^2=0.9983$.

At P3, both SR101-positive ($n=42$) and SR101-negative ($n=13$) cells exhibited voltage-activated outward currents and only non-linear *I/V* relationships with a variable degree of outward rectification were found (“non-passive cells”, nPC; Figs. 3A, D and 4A, B). In SR101-positive cells, outward-currents were non-inactivating (Fig. 3A), while in SR101-negative cells, the amplitude of outward currents decreased over time (Fig. 4A). At P7, SR101-positive cells exhibited non-linear *I/V* relationships with non-inactivating outward currents as well ($n=6$; Fig. 3B and D), whereas the majority (78%) of SR101-positive cells at P15 ($n=38$) and all SR101-positive cells at P24–27 ($n=13$) lacked voltage-gated currents and thus showed a linear *I/V* relationship (“passive cells”, PC; Figs. 3C, D and 4D). SR101-negative cells at P15 ($n=5$) as well as at P24–27 ($n=6$), in contrast, exclusively showed non-linear properties (Fig. 4C).

To further characterize SR101-positive and negative cells, we examined which phenotype functionally expressed voltage-gated fast inward currents. To relieve inactivation of voltage-gated Na⁺ channels, the voltage step protocol was extended by a hyperpolarizing preconditioning pulse to -120 mV. SR101-positive cells completely lacked fast inward currents at P3 ($n=42$; Fig. 4B), at P15 ($n=37$; Fig. 4D) as well as at P24–27 ($n=13$). In contrast, 4 out of 13 SR101-negative cells at P3 (Fig. 4A) and all SR101-negative cells at P15 ($n=5$) and at P24–27 ($n=6$) expressed voltage-gated fast inward currents.

Taken together, these results demonstrate that small-sized, SBFI-stained cells in the *stratum radiatum* represent glial cells that can be divided into two subtypes differing in their staining pattern with SR101 as well as in their passive and active membrane properties. At P15 and in young adults, the vast majority of SR101-positive cells show the typical electrophysiological properties of classical passive astrocytes (Bordey and Sontheimer, 2000; D’Ambrosio et al., 1998; Steinhauser et al., 1992; Zhou et al., 2006).

3.3. Immunohistochemical characterization of SR101-positive cells

To further establish the astrocytic identity of SR101-positive glial cells at P15, we immunohistochemically stained for GFAP. To this end, SR101-positive cells were first characterized electrophysiologically and in parallel filled with the fluorescent dye Alexa 488 via the patch pipette to enable their identification in the slices processed for immunohistochemistry. As described above, we found that all SR101-positive cells at P15 exhibited electrophysiological properties of classical astrocytes ($n=26$). The majority of these cells ($n=23/26$ cells) were also GFAP-positive, confirming their astrocytic identity (Fig. 5A). Three of 26 investigated SR101-positive cells were GFAP-negative (Fig. 5B), indicating that GFAP only labels a subset of astroglial cells as reported earlier (Lee et al., 2006; Raponi et al., 2007).

3.4. ATP-induced Ca²⁺ transients in SR101-stained slices

To validate the described double-staining protocol of SR101 and ion-selective dyes for physiological measurements, we performed dynamic fluorescence imaging in acute hippocampal slices at P15, employing the Ca²⁺-sensitive dye Fura-2-AM (Fig. 6). We tested the responses of the cells to a focal pressure application of ATP (10 μM for 100 ms) through a fine micropipette, which has been shown to induce intracellular Ca²⁺ transients in glial cells (Verkhatsky et al., 1998). Focal applica-

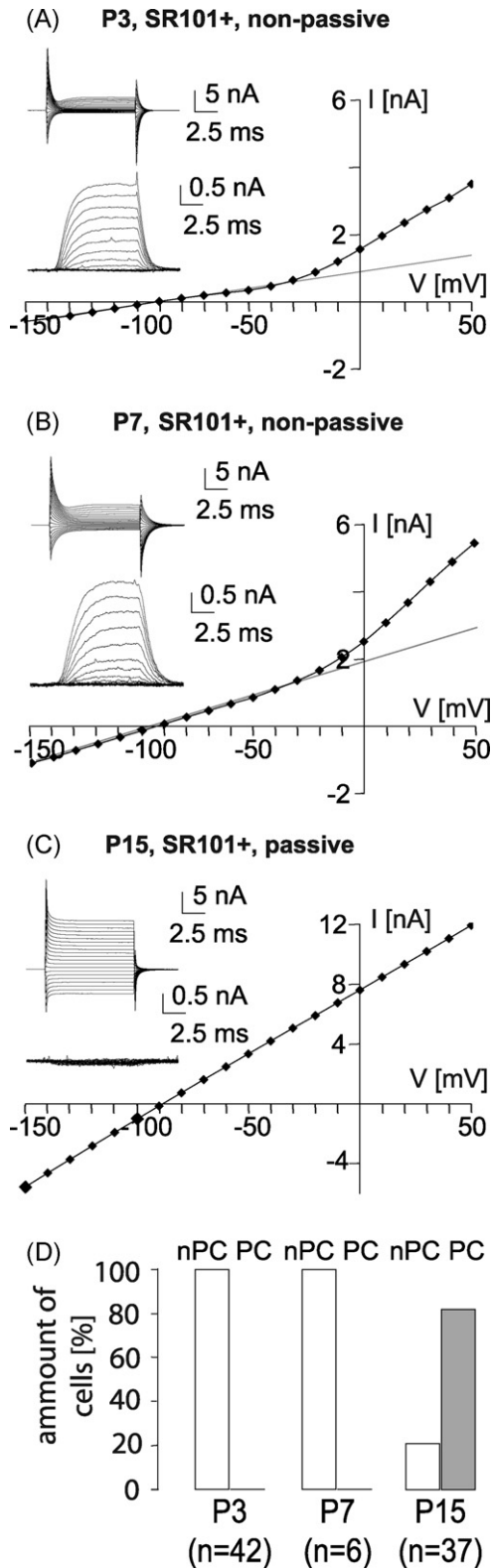


Fig. 3. *I/V* relationship of SR101-positive cells of P3 (A), P7 (B) and P15 (C) rats. Cells were held at -85 mV and subjected to 10 ms voltage steps ranging from -150 to $+50$ mV at 10 mV increments. The insets on the left side show the resulting membrane currents before (top) and after leak subtraction (bottom). The *I/V* plots depict the amplitudes of the resulting currents at 8–10 ms after the start of the voltage step of the same cells, the grey lines show the linear regression curves. Animals at P3 (A) and P7 (B) exclusively showed non-linear

tion of ATP resulted in a transient elevation of the intracellular Ca^{2+} concentration in 15 out of 18 SR101-positive (83%), as well as in 5 out of 7 SR101-negative cells (71%) within the field of view ($n=6$ experiments in 6 slices; Fig. 6). The amplitude of ATP-induced calcium transients was dependent on the distance of the cells from the tip of the application pipette, the orientation of perfusion flow, and the depth of the cell in the slice. When analyzing cells located within a circular area with a radius of $50 \mu\text{m}$ from the tip of the application pipette, the amplitude of the calcium transients was not significantly different between SR101-positive and SR101-negative cells and averaged about 20 nM. In summary, these measurements confirm that SR101 labeling of acute slices does not interfere with intracellular ion measurements using ion-selective fluorescent dyes (Jourdain et al., 2007; Nimmerjahn et al., 2004).

4. Discussion

In the present study, we describe a procedure for double-labeling of acute slice preparations of the rat hippocampus with the fluorescent dye SR101 and AM-esters of ion-selective fluorescent dyes. SR101 was introduced recently to selectively identify astrocytes in the neocortex of 2–4-week-old rats (Nimmerjahn et al., 2004). It is a red fluorescent dye that can be combined with fluorescent dyes excited in the UV range such as Fura-2 or SBFI (this study) or excited at 400–500 nm such as Oregon Green (Nimmerjahn et al., 2004) and Alexa 488 (this study, Nimmerjahn et al., 2004). In accordance with the latter study, we did not find any evidence for a distortion of induced intracellular Ca^{2+} transients in cells that were stained with both, SR101 and the ion-selective fluorescent dye.

Astrocytes *in situ* are heterogeneous with respect to their physiological properties (D'Ambrosio et al., 1998; Grass et al., 2004; Matthias et al., 2003; Steinhauser et al., 1992, 1994b; Zhou and Kimelberg, 2000, 2001) and undergo considerable changes in channel complement and passive membrane properties during early postnatal development (Bordey and Sontheimer, 1997; Kressin et al., 1995; Zhou et al., 2006). Thus, using whole-cell patch-clamp, imaging techniques and immunohistochemistry, we characterized the properties of SR101-positive versus SR101-negative cells in the *stratum radiatum* at postnatal days 3, 7, 15 and 24–27.

Based on their electrophysiological properties, two basic types of astrocytes have been described in the hippocampus (Bordey and Sontheimer, 2000; D'Ambrosio et al., 1998; Kressin et al., 1995; Steinhauser et al., 1994b; Zhou and Kimelberg, 2001). One cell type, termed “outwardly rectifying” (Zhou and Kimelberg, 2000, 2001) or “complex” (Kressin et al., 1995; Steinhauser et al., 1994b) is mainly characterized by a membrane potential which is significantly more positive than the equilibrium potential for K^+ , by a high input resistance, and by a low membrane capacity. Moreover, this cell type functionally

I/V relationships, in P15 animals (C), mostly linear *I/V* curves were found. (D) Quantification of the amount of cells with non-linear (non-passive cells, nPCs, white bars) or linear (passive cells, PCs, grey bars) *I/V* curves on the total number of SR101-positive cells at P3, P7 and P15.

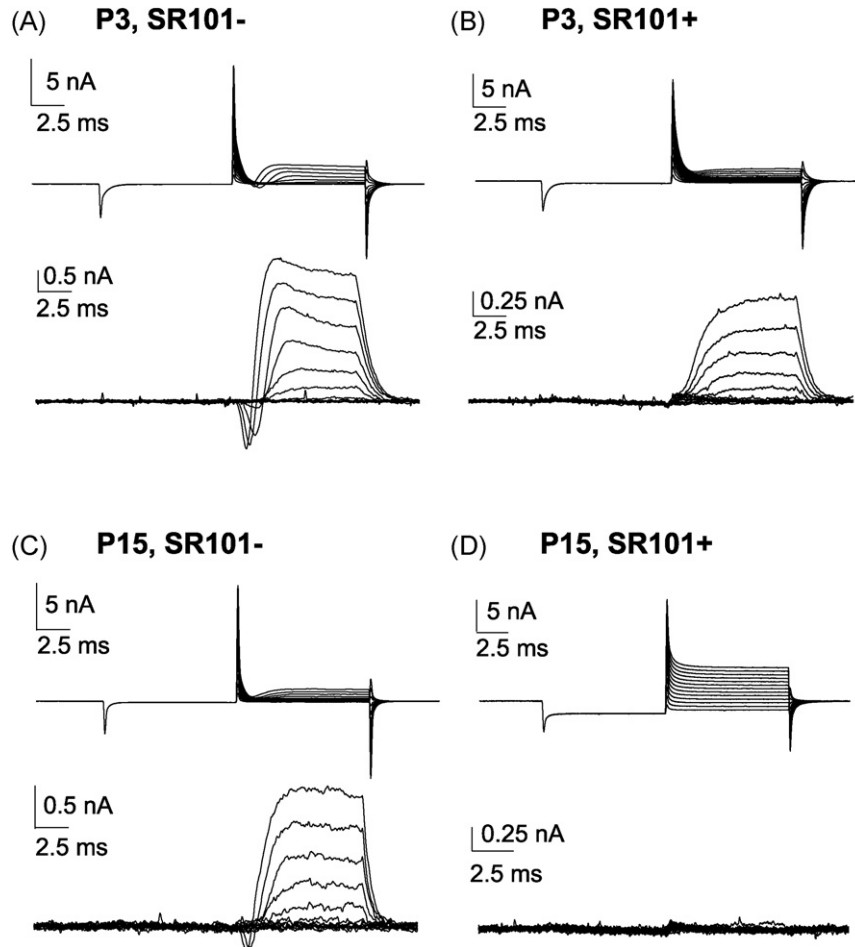


Fig. 4. Expression pattern of voltage-gated fast inward currents at P3 (A, B) and P15 (C, D). To relieve inactivation of voltage-gated Na^+ channels, cells were held at -85 mV and subjected to a prepulse to -120 mV for 10 ms before stepping from -110 to $+10$ mV in increments of 10 mV. Shown are the resulting currents before (upper traces) and after (lower traces) leak subtraction. At both ages, fast voltage-gated inward currents were only observed in SR101-negative (A, C), but not in SR101-positive (B, D) cells.

expresses two types of K^+ -outward currents, a delayed rectifier and a transient A-type current, as well as TTX-sensitive Na^+ channels. The hallmarks of the second type of astrocytes are a highly negative membrane potential, a low input resistance, and a high membrane capacity. Furthermore, these cells lack voltage-gated Na^+ currents and show a largely symmetrical expression of inward and outward K^+ currents that consist predominantly of ohmic currents with small contributions of delayed rectifier K^+ currents. Accordingly, this cell type was called “passive” (Kressin et al., 1995; Steinhauser et al., 1994a) or “variably rectifying” (Zhou and Kimelberg, 2000, 2001) astrocyte. In addition, both astrocyte types differ in their expression profile for ionotropic glutamate receptors and glutamate transporters. Whereas the first type expresses ionotropic glutamate receptors and lacks glutamate transporter currents (Matthias et al., 2003; Zhou and Kimelberg, 2001), the second type lacks ionotropic glutamate receptors, but shows significant glutamate uptake currents (Matthias et al., 2003; Zhou and Kimelberg, 2001). Based on these differences, the second type (“passive” or “variably rectifying” astrocyte) is often regarded as the “classical” astrocyte, as it is capable to perform classical functions of astrocytes, such as the uptake of glutamate and potassium from the

extracellular space (Matthias et al., 2003; Zhou and Kimelberg, 2001).

Our results show that SR101-positive cells during the first 4 weeks of postnatal development display the electrophysiological properties typical for immature and mature classical astrocytes described above. The developmental profile of current expression of SR101-positive cells is in good agreement with earlier studies showing that the amount of outward rectification in such cells decreases with age (Steinhauser et al., 1992; Wallraff et al., 2004; Zhou et al., 2006). The electrophysiological properties of SR101-negative cells, in contrast, are reminiscent of the first type of astrocytes described above, but may also include a population of glial cells positive for the chondroitin sulfate proteoglycan NG2 and thus, may partly represent glial progenitor cells (Matthias et al., 2003; Zhou et al., 2006).

Taken together, our data demonstrate for the first time that SR101, in contrast to conventional fluorescent ion-selective dyes such as Fura-2 or SBFI, selectively labels a subpopulation of glial cells in the early postnatal hippocampus that shows the typical developmental changes and characteristics of classical astrocytes. Staining with SR101 enables a direct and reliable identification of virtually all such astrocytes in acute brain slices

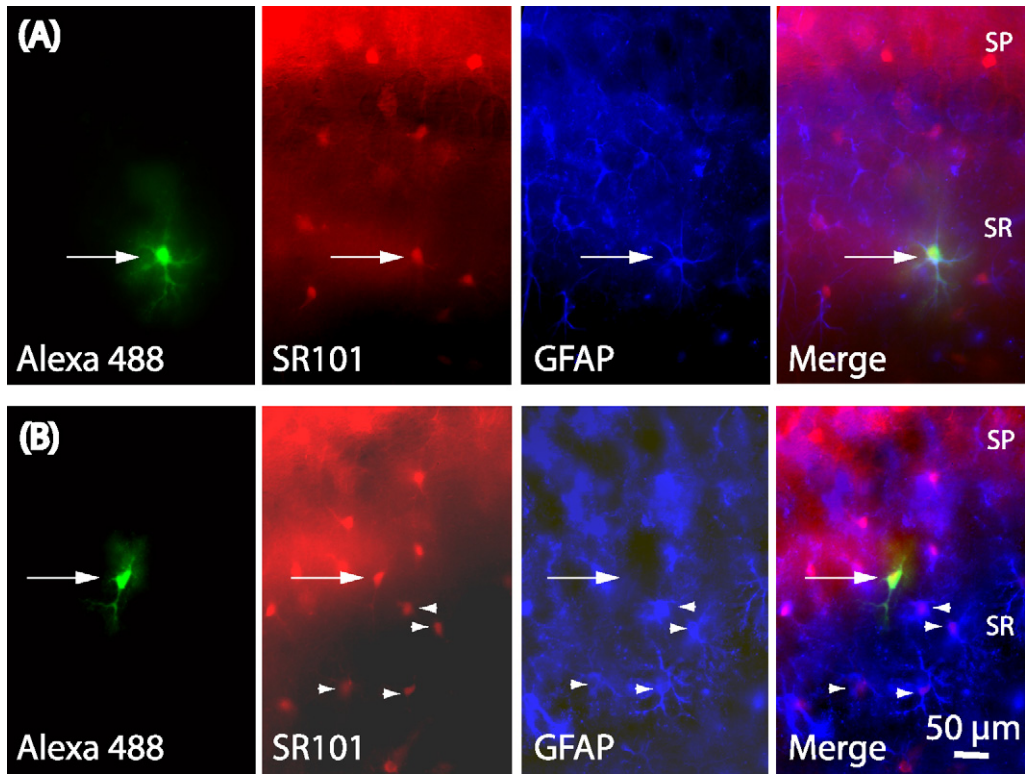


Fig. 5. Immunohistochemical characterization of SR101-positive cells at P15. (A) From left to right: image of the staining pattern of SR101 in the *stratum radiatum*. Based on this staining, a SR101-positive cell was chosen (arrow) and characterized electrophysiologically while filling the cell with Alexa 488. In the subsequent immunohistochemical analysis, the same cell also showed immunoreactivity for GFAP. The merged picture of all three fluorescence images confirms the identity of the triple-labeled cell. (B) The same experimental design also identified a cell which was SR101-positive, electrophysiologically characterized as glial cell, but showed no immunoreactivity for GFAP (arrow). The arrowheads point to cells, which were double-labeled for SR101 and GFAP. SP: *stratum pyramidale*; SR: *stratum radiatum*.

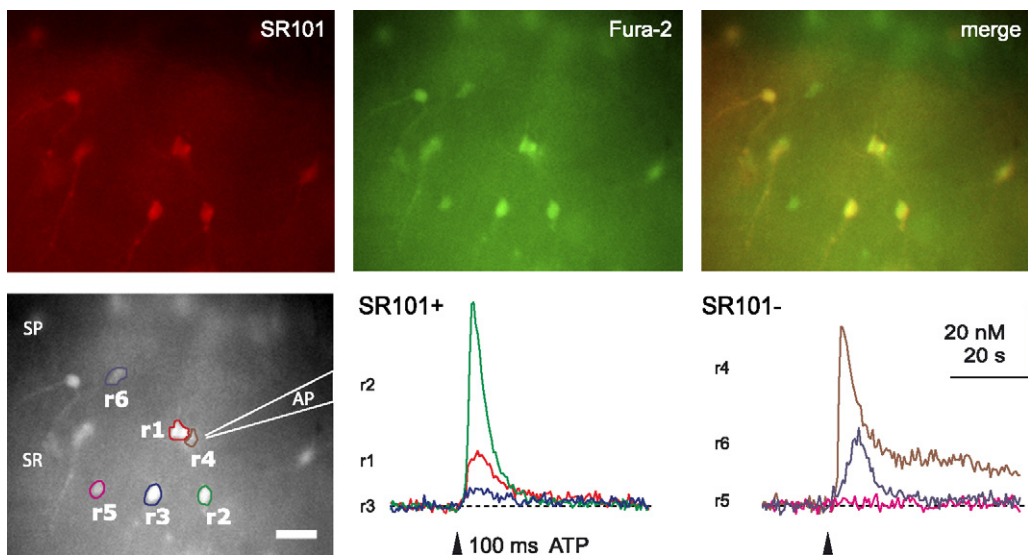


Fig. 6. ATP-induced Ca^{2+} transients in SR101-positive and SR101-negative cells at P15. Top, left: image of the staining pattern of SR101 in the *stratum radiatum*. Top, center and right: staining pattern of the Ca^{2+} -sensitive dye Fura-2 and merged image. Bottom, left: image of the Fura-2 fluorescence. The colored lines indicate the regions of interest (r1–r6) in which the Ca^{2+} -measurements were performed. The position of the application pipette (AP) is indicated schematically on the right. Bottom, right: focal pressure application of 10 μ M ATP for 100 ms induced Ca^{2+} transients in both SR101-positive (left) and SR101-negative (right) cells. The experiment was performed using a widefield imaging system.

for physiological measurements as well as immunohistochemical studies. Owing to its reliability and uncomplicated handling, we expect that this technique will be helpful in future investigations studying the functions of astrocytes and neuron-glia interaction in the developing brain.

Acknowledgements

We thank Simone Durry and Claudia Roderigo for expert technical assistance. This study was supported by the DFG.

References

- Araque A, Parpura V, Sanzgiri RP, Haydon PG. Tripartite synapses: glia, the unacknowledged partner. *Trends Neurosci* 1999;22:208–15.
- Bordey A, Sontheimer H. Postnatal development of ionic currents in rat hippocampal astrocytes in situ. *J Neurophysiol* 1997;78:461–77.
- Bordey A, Sontheimer H. Ion channel expression by astrocytes in situ: comparison of different CNS regions. *Glia* 2000;30:27–38.
- Dallwig R, Deitmer JW. Cell-type specific calcium responses in acute rat hippocampal slices. *J Neurosci Methods* 2002;116:77–87.
- D'Ambrosio R, Wenzel J, Schwartzkroin PA, McKhann II GM, Janigro D. Functional specialization and topographic segregation of hippocampal astrocytes. *J Neurosci* 1998;18:4425–38.
- Fiacco TA, Agulhon C, Taves SR, Petravic J, Casper KB, Dong X, et al. Selective stimulation of astrocyte calcium in situ does not affect neuronal excitatory synaptic activity. *Neuron* 2007;54:611–26.
- Grass D, Pawlowski PG, Hirrlinger J, Papadopoulos N, Richter DW, Kirchhoff F, et al. Diversity of functional astroglial properties in the respiratory network. *J Neurosci* 2004;24:1358–65.
- Haydon P. Glia: listening and talking to the synapse. *Nat Neurosci Rev* 2001;2:185–93.
- Haydon PG, Carmignoto G. Astrocyte control of synaptic transmission and neurovascular coupling. *Physiol Rev* 2006;86:1009–31.
- Hirrlinger PG, Scheller A, Braun C, Hirrlinger J, Kirchhoff F. Temporal control of gene recombination in astrocytes by transgenic expression of the tamoxifen-inducible DNA recombinase variant CreERT2. *Glia* 2006;54:11–20.
- Jourdain P, Bergersen LH, Bhaukaurally K, Bezzi P, Santello M, Domercq M, et al. Glutamate exocytosis from astrocytes controls synaptic strength. *Nat Neurosci* 2007;10:331–9.
- Kafitz KW, Greer CA. Differential expression of extracellular matrix and cell adhesion molecules in the olfactory nerve and glomerular layers of adult rats. *J Neurobiol* 1998;34:271–82 [published erratum appears in *J Neurobiol* 1998 Apr;35(1):118].
- Kafitz KW, Guttinger HR, Muller CM. Seasonal changes in astrocytes parallel neuronal plasticity in the song control area HVC of the canary. *Glia* 1999;27:88–100.
- Kang J, Jiang L, Goldman S, Nedergaard M. Astrocyte-mediated potentiation of inhibitory synaptic transmission. *Nat Neurosci* 1998;1:683–92.
- Kimelberg HK. The problem of astrocyte identity. *Neurochem Int* 2004;45:191–202.
- Kressin K, Kuprijanova E, Jabs R, Seifert G, Steinhauser C. Developmental regulation of Na⁺ and K⁺ conductances in glial cells of mouse hippocampal brain slices. *Glia* 1995;15:173–87.
- Lee Y, Su M, Messing A, Brenner M. Astrocyte heterogeneity revealed by expression of a GFAP-LacZ transgene. *Glia* 2006;53:677–87.
- Matthias K, Kirchhoff F, Seifert G, Huttmann K, Matyash M, Kettenmann H, et al. Segregated expression of AMPA-type glutamate receptors and glutamate transporters defines distinct astrocyte populations in the mouse hippocampus. *J Neurosci* 2003;23:1750–8.
- Meier SD, Kovalchuk Y, Rose CR. Properties of the new fluorescent Na⁺ indicator CoroNa Green: comparison with SBFI and confocal Na⁺ imaging. *J Neurosci Methods* 2006;155:251–9.
- Metea MR, Newman EA. Glial cells dilate and constrict blood vessels: a mechanism of neurovascular coupling. *J Neurosci* 2006;26:2862–70.
- Mulligan SJ, MacVicar BA. Calcium transients in astrocyte endfeet cause cerebrovascular constrictions. *Nature* 2004;431:195–9.
- Nedergaard M. Direct signaling from astrocytes to neurons in cultures of mammalian brain cells. *Science* 1994;263:1768–71.
- Newman EA, Volterra A. Glial control of synaptic function. *Glia* 2004;47:207–8.
- Nimmerjahn A, Kirchhoff F, Kerr JN, Helmchen F. Sulforhodamine 101 as a specific marker of astroglia in the neocortex in vivo. *Nat Methods* 2004;1:31–7.
- Nolte C, Matyash M, Pivneva T, Schipke CG, Ohlemeyer C, Hanisch UK, et al. GFAP promoter-controlled EGFP-expressing transgenic mice: a tool to visualize astrocytes and astrogliosis in living brain tissue. *Glia* 2001;33:72–86.
- Parri HR, Gould TM, Crunelli V. Spontaneous astrocytic Ca²⁺ oscillations in situ drive NMDAR-mediated neuronal excitation. *Nat Neurosci* 2001;4:803–12.
- Parri R, Crunelli V. Astrocytes target presynaptic NMDA receptors to give synapses a boost. *Nat Neurosci* 2007;10:271–3.
- Pascual O, Casper KB, Kubera C, Zhang J, Revilla-Sanchez R, Sul JY, et al. Astrocytic purinergic signaling coordinates synaptic networks. *Science* 2005;310:113–6.
- Raponi E, Agenes F, Delphin C, Assard N, Baudier J, Legraverend C, et al. S100B expression defines a state in which GFAP-expressing cells lose their neural stem cell potential and acquire a more mature developmental stage. *Glia* 2007;55:165–77.
- Rose CR, Ransom BR. Intracellular Na⁺ homeostasis in cultured rat hippocampal astrocytes. *J Physiol* 1996;491:291–305.
- Rose CR, Ransom BR. Gap junctions equalize intracellular Na⁺ concentration in astrocytes. *Glia* 1997;20:299–307.
- Schipke CG, Kettenmann H. Astrocyte responses to neuronal activity. *Glia* 2004;47:226–32.
- Serrano A, Haddjeri N, Lacaille JC, Robitaille R. GABAergic network activation of glial cells underlies hippocampal heterosynaptic depression. *J Neurosci* 2006;26:5370–82.
- Steinhauser C, Berger T, Frotscher M, Kettenmann H. Heterogeneity in the membrane current pattern of identified glial cells in the hippocampal slice. *Eur J Neurosci* 1992;4:472–84.
- Steinhauser C, Jabs R, Kettenmann H. Properties of GABA and glutamate responses in identified glial cells of the mouse hippocampal slice. *Hippocampus* 1994a;4:19–35.
- Steinhauser C, Kressin K, Kuprijanova E, Weber M, Seifert G. Properties of voltage-activated Na⁺ and K⁺ currents in mouse hippocampal glial cells in situ and after acute isolation from tissue slices. *Pflugers Arch* 1994b;428:610–20.
- Stosiek C, Garaschuk O, Holthoff K, Konnerth A. In vivo two-photon calcium imaging of neuronal networks. *Proc Natl Acad Sci USA* 2003;100:7319–24.
- Takano T, Tian GF, Peng W, Lou N, Libionka W, Han X, et al. Astrocyte-mediated control of cerebral blood flow. *Nat Neurosci* 2006;9:260–7.
- Verkhratsky A, Orkand RK, Kettenmann H. Glial calcium: homeostasis and signaling function. *Physiol Rev* 1998;78:99–141.
- Volterra A, Meldolesi J. Astrocytes, from brain glue to communication elements: the revolution continues. *Nat Rev Neurosci* 2005;6:626–40.
- Wallraff A, Odermatt B, Willecke K, Steinhauser C. Distinct types of astroglial cells in the hippocampus differ in gap junction coupling. *Glia* 2004;48:36–43.
- Wang X, Lou N, Xu Q, Tian GF, Peng WG, Han X, et al. Astrocytic Ca(2+) signaling evoked by sensory stimulation in vivo. *Nat Neurosci* 2006;9:816–23.
- Zhou M, Kimelberg HK. Freshly isolated astrocytes from rat hippocampus show two distinct current patterns and different [K(+)](o) uptake capabilities. *J Neurophysiol* 2000;84:2746–57.
- Zhou M, Kimelberg HK. Freshly isolated hippocampal CA1 astrocytes comprise two populations differing in glutamate transporter and AMPA receptor expression. *J Neurosci* 2001;21:7901–8.
- Zhou M, Schools GP, Kimelberg HK. Development of GLAST(+) astrocytes and NG2(+) glia in rat hippocampus CA1: mature astrocytes are electrophysiologically passive. *J Neurophysiol* 2006;95:134–43.
- Zhuo L, Sun B, Zhang CL, Fine A, Chiu SY, Messing A. Live astrocytes visualized by green fluorescent protein in transgenic mice. *Dev Biol* 1997;187:36–42.
- Zonta M, Angulo MC, Gobbo S, Rosengarten B, Hossmann KA, Pozzan T, et al. Neuron-to-astrocyte signaling is central to the dynamic control of brain microcirculation. *Nat Neurosci* 2003;6:43–50.